Journal of Molecular Liquids 408 (2024) 125045

Contents lists available at ScienceDirect

Journal of Molecular Liquids

journal homepage: www.elsevier.com/locate/molliq

Theoretical and experimental study of a new antioxidant xanthone: Solvent and intramolecular hydrogen bond effects

N.S.S. dos Santos [a], H.B. Barbieri [b], M. Pinheiro [a,b], T.P. Fill [b], M.H. Queiroz [c], J. Pina [d], E. Belo [e], H.C. Georg [f], A.R. da Cunha [g,h], P.S.B. Marinho [d], A.M.R. Marinho [d], K. Coutinho [h], S. Canuto [h], R. Gester [h,i,*]

[a] Programa de Pós-Graduação em Química, Universidade Federal do Sul e Sudeste do Pará, 68507-590, Marabá PA, Brazil
[b] Instituto de Química, Universidade Estadual de Campinas, 13083-862, Campinas SP, Brazil
[c] Instituto de Química, Universidade Federal da Bahia, Campus de Ondina, 40170-115, Salvador BA, Brazil
[d] Programa de Pós-graduação em Química, Universidade Federal do Pará, 66075-110, Belém PA, Brazil
[e] Faculdade de Física, Campus Universitário de Tucuruí, Universidade Federal do Pará, 68464-000, Tucurui PA, Brazil
[f] Instituto de Física, Universidade Federal de Goiás, 74690-900, Goiânia GO, Brazil
[g] Universidade Federal do Maranhão, UFMA, Campus Balsas, CEP 65800-000, Maranhão, Brazil
[h] Instituto de Física, Universidade de São Paulo, Rua do Matão 1371, 05588-090, São Paulo SP, Brazil
[i] Faculdade de Física, Universidade Federal do Sul e Sudeste do Pará, 68507-590, Marabá PA, Brazil

ARTICLE INFO

Keywords:
Xanthones
Antioxidant
DFT
Solvent effects
Hydrogen bonds

ABSTRACT

Free radicals are harmful reactive species that cause various problems in the human body. Antioxidant compounds, such as xanthones found in natural products, can help prevent these effects. This study focuses on the antioxidant behavior of ravenelin (RVL) and ravenelin B (RVLB), a newly discovered xanthone in the *Exserohilum rostratum* fungus. Both experimental and *in silico* tests were conducted, comparing them to ascorbic acid, a standard antioxidant. The results showed that RVL has a lower bond dissociation energy (312 kJ/mol) than ascorbic acid (313 kJ/mol), indicating comparable antioxidant performance. This difference is mild but agrees with the experiment that indicates RVL efficiency is equivalent to ascorbic acid at low concentrations. RVLB, however, demands higher dissociation energy (323 kJ/mol) and consequently it has a lower antioxidative efficiency. Thus, antioxidant capacity is found as RVL > ascorbic acid > RVLB. From experimental assays, the RVL performance was confirmed through experimental tests at different solute concentrations. The study also examines the effects of solvents and intramolecular hydrogen bonds. Ravenelin molecules present three hydroxyl groups involved in intramolecular OH···O interactions. However, analysis based on the infrared spectra, as well as Bader's theory and non-covalent interactions done in water solvent showed that the two strongest H-bonds (≈ −37 kJ/mol) better stabilize the molecular structure, but are not favorable to antioxidant reactions, indicating that hydrogen scavenging occurs at the less hydrogen-bonded hydroxyl group. The solvent also plays an active role first in facilitating hydrogen abstraction besides changing the hydrogen scavenging mechanism according to the environmental polarizability. Additionally, the antioxidant mechanism of ravenelin molecules changes from nonpolar to polar solvents, allowing for hydrogen abstraction.

1. Introduction

In excess, free radicals are harmful to living organisms, causing premature aging of all organic tissues that make up the human body [1]. As a natural defense, living organisms can take advantage of enzymes capable of neutralizing these radicals. However, unhealthy habits such as smoking, excessive alcohol consumption, and sun exposure, among other factors, can disrupt this balance. In this context, antioxidant substances gain special relevance. These natural products, primarily extracted from fruits and medicinal plants [2], are beneficial to living organisms once they are capable of undergoing a simple chemical reaction, losing hydrogen atoms to neutralize free radicals. Thus, these compounds are of great interest to the pharmaceutical and food industries.

* Corresponding author.
E-mail address: gester@unifesspa.edu.br (R. Gester).

https://doi.org/10.1016/j.molliq.2024.125045
Received 9 February 2024; Received in revised form 6 May 2024; Accepted 16 May 2024
Available online 27 May 2024

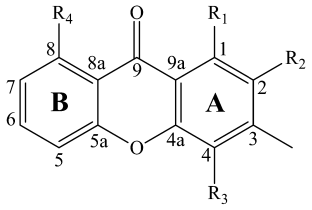

RVL - R_1, R_3, R_4 = OH; R_2 = H
RVLB - R_1, R_2, R_4 = OH; R_3 = H

Fig. 1. Representation of ravenelin (RVL) and ravenelin B (RVLB). These compounds are isomers of position differing the reallocation of the OH group from position 4 in RVL to 2 in RVLB.

In the search for new antioxidant compounds, molecular modeling techniques and quantum chemical approximations play an important role in providing information that is not easily obtained through experimental techniques [3–5].

For example, theory shows that the hydrogen atom transfer process can occur in three different forms. Therefore, besides being possible to determine the most likely molecular site for hydrogen removal, it is equally feasible to identify the dominant mechanism of antioxidant behavior and the conditions that affect these processes. In a series of recent reports, for instance, it has been shown that the simple inclusion of the solvent is enough to change the oxidative mechanism observed in gas phase [3,6,7]. These discoveries reveal that the environment is an important factor in the study of antioxidant molecules.

In a recent discussion, ravenelin (1,4,8-trihydroxy-3-methyl-9H-xanthen-9-one) has been identified and extracted from the endophytic fungus *Exserohilum rostratum* and tested with success against Gram-positive bacteria strains [8].

In addition, Marinho and collaborators recently identified ravenelin B (1,2,8-trihydroxy-3-methyl-9H-xanthen-9-one), a new xanthone present in the same fungus. From Fig. 1, it is evident that both RVL and RVLB are positional isomers, with OH and CH_3 groups that can participate in antioxidant reactions. However, despite xanthones being associated with diverse biological functions, no research has been conducted to explore the antioxidant potential of RVL and RVLB molecules.

In the face of the discussion above, we have carried out a systematic investigation of the antioxidant activity of ravenelin molecules coupling experimental and theoretical methodologies. Once a sufficient amount of RVL can be extracted from the *Exserohilum rostratum* fungus, antioxidant assays are conducted specifically for this compound. Additionally, quantum chemical methods are employed to investigate its antioxidant properties. Subsequently, molecular modeling techniques are used to compare RVL and RVLB performances. As a general finding, both compounds might be promising in the pharmacological industry. The results also show that the polarity of the solvent and the intramolecular hydrogen bond formations play fundamental roles, selecting the antioxidant mechanism, reducing the energetic cost of the hydrogen abstraction, and vitalizing the removal of free radicals from the human organism.

2. Methodology

2.1. Experimental

2.1.1. Isolation of ravenelin

Ravenelin (Fig. 1a) used in this work was isolated from the fungal biomass of *E. rostratum*, deposited at National Genetic Heritage and Associated Traditional Knowledge Management System (SisGen) under the accession number AFE3E98. The fungus cultivation, isolation and structural characterization are described elsewhere [8].

2.1.2. Ravenelin antioxidant assay

The 2,2-diphenyl-1-picrylhydrazyl (DPPH) antioxidant assay involves assessing the ability of antioxidant compounds to capture free radicals [11,12]. In this study, we compared the antioxidant capacity of ravenelin with that of ascorbic acid, a widely recognized antioxidant. Both compounds were evaluated in a concentration range of 100 – 6.25 ppm, prepared from a 100 ppm stock solution (**Table S1**). Samples were prepared in triplicate, and the final sample volume, after the addition of the DPPH solution (40 ppm), was 2 mL.

Following the addition of the DPPH solution, the samples were stored under ambient conditions without exposure to light for 30 minutes at room temperature. Absorbance was measured at a wavelength of 518 nm using a Zenyth 200rt Microplate Reader and Spectrophotometer. The calculation of antioxidant capacity will be determined by the difference between the control absorbance ($A_{control}$) and the sample absorbance (A_{sample}) described as:

$$\%\ \text{antioxidant capacity} = \frac{A_{control} - A_{sample}}{A_{control}} \times 100 \quad (1)$$

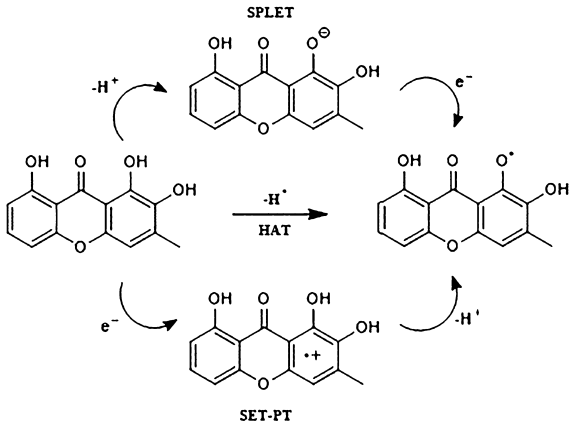

Fig. 2. Antioxidant mechanisms of new xanthone: Hydrogen atom transfer (HAT), Sequential proton loss electron transfer (SPLET) and Single electron transfer followed by proton transfer (SET-PT).

2.2. Theoretical

The *in silico* discussion of the antioxidant behavior of ravenelin and ravenelin B is entirely based on a thermochemical analysis. In this context, the enthalpy (**H**) is the main parameter, and is obtained from the vibrational frequencies of the optimized molecular geometries. According to theory, the hydrogen transfer process can occur under three different manners [16] as shown in Fig. 2, and the viability of one of these reactions is estimated by computing the energetic difference between the final and initial enthalpies. The first reactive mechanism is the Hydrogen Atom Transfer (HAT), which occurs in a single step with the complete removal of the hydrogen atom. This mechanism is described by the Bond Dissociation Enthalpy (BDE) as:

$$BDE = H^{\bullet}_{ArO} + H^{\bullet}_{H} - H_{ArOH} \quad (2)$$

On the other hand, the second mechanism, SET-PT (Sequential Electron Transfer - Proton Transfer), happens in two steps. In this particular case, an electron transfer occurs first, being followed by a proton migration to the free radical. In this order, this procedure described by the Adiabatic Ionization Potential (AIP) and Proton Dissociation Enthalpy (PDE) as:

$$AIP = H^{\bullet+}_{ArOH} + H_{e} - H_{ArOH} \quad (3)$$

$$PDE = H^{\bullet}_{ArO} + H^{+}_{H} - H^{\bullet+}_{ArOH} \quad (4)$$

Finally, the third and last mechanism, SPLET (Sequential Proton Loss Electron Transfer), is the reverse of the previous one. In this case, first the system loses the proton, and subsequently occurs an electron trans-

fer. This mechanism is described by Proton Affinity (PA) and Electron Transfer Enthalpy (ETE) as:

$$PA = H^{-}_{ArO} + H^{+}_{H} - H_{ArOH} \quad (5)$$

$$ETE = H^{\bullet}_{ArO} + H_{e} - H^{-}_{ArO} \quad (6)$$

All molecular geometries used in the thermochemical analysis were obtained within the framework of DFT using the B3LYP method [17–19] with the 6-311++G(2p, 2d) basis set [20,21], and the Integral-Equation Formalism of the Polarizable-Continuum Model (IEF-PCM) [22] used to take the solvent effect into account when necessary. Moreover, for the open-shell systems (radicals and cations), the unrestricted formalism was applied, and the absence of negative frequencies in the vibrational spectra confirmed that the molecular geometries correspond to minimum energy geometries. Besides, it is important to mention that all quantum mechanics calculations were performed using the Gaussian 16 program [23]. Additionally, the recommended enthalpies for electrons, protons, and hydrogen (see **Table S2**) have been previously assigned by Urbaniak and collaborators [24].

The intramolecular H-bonds were characterized using the Bader's Atoms in molecules (AIM) [25–27] and non-covalent interactions (NCI) [28,29] theories, respectively. We have found the bond critical points (BCPs) using AIM through the electron density $\rho(r)$. In the case of the NCI, the reduced density gradient, $s = \frac{1}{2(3^2)^{1/3}} \frac{\rho(r)}{r^{4/3}}$, and the second eigenvalue, λ_2 of the Hessian of the $\rho(r)$ were used to characterize the non-covalent interactions. In this sense, the colors blue, green and red represent strong, weak and repulsive interactions, respectively. The AIM and NCI analysis was performed using the Multiwfn program [30]. Additionally, the molecular graphs have been constructed by using the VMD program [31].

Finally, a comment about the choice of the structures in the face of molecular tautomerism. In principle, xanthones can oscillate between their keto and enol structures. This tautomerism depends on several variables. However, we held our focus on the keto form once many results indicated that in polar solvents, this structure better stabilizes [32–34].

3. Results

3.1. Antioxidant analysis

The DPPH assay is commonly used to assess the potential of an antioxidant molecule to capture free radicals [9]. It is considered a standard and straightforward colorimetric method for evaluating the antioxidant properties of compounds. DPPH is a stable radical that appears purple in solution, absorbs UV-Vis radiation in the wavelength range of 515-518 nm [35]. The assay is based on the principle that DPPH accepts a hydrogen atom from an antioxidant compound, reducing it from DPPH$^{\bullet}$ to DPPH2. The reduction leads to color alteration to yellow, and the absorbance in the region between 515-518 nm decreases [13].

Ascorbic acid is an efficient antioxidant that eliminates toxic free radicals and other reactive oxygen species (ROS) formed during cellular metabolism [10,11]. It is considered effective for cells in nearly all aerobic organisms. Therefore, ascorbic acid, along with other compounds such as gallic acid, butylated hydroxytoluene (BHT), and butylated hydroxyanisole (BHA), is used as a reference standard for antioxidant activity assays with DPPH [13].

In this study, we compared the antioxidant capacity of ravenelin with that of ascorbic acid (Table 1). The results indicate that, at the higher concentrations tested (100 and 50 ppm), ascorbic acid exhibited a significantly higher antioxidant capacity than ravenelin (*p-value* < 0.0001) (Fig. 3). These findings can be attributed to the low water solubility of ravenelin [14]. This probably influenced the scattering of light and interfered with the spectrophotometric analysis.

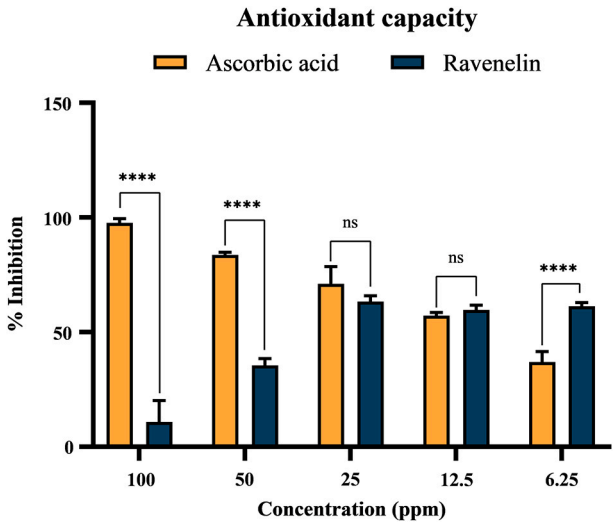

Fig. 3. The percentage of antioxidant capacity for ascorbic acid and ravenelin across the tested concentration range (100 – 6.25 ppm). ANOVA analysis with Sidak's multiple comparisons test was conducted to assess the antioxidant capacities of both compounds at each tested concentration. Statistical significance levels are denoted as follows: ns - *p-value* > 0.05; * - *p-value* < 0.05; ** - *p-value* < 0.01; *** - *p-value* < 0.001; **** - *p-value* < 0.0001.

Table 1
Mean values of absorbance for ravenelin and ascorbic acid at 518 nm for the tested concentrations and the mean percentage of antioxidant capacity.

Compound	Concentration (ppm)	Absorbance	Antioxidant capacity (%)
Ravenelin	100	0.1940	10.84
	50	0.1493	35.54
	25	0.0850	63.31
	12.5	0.0933	59.71
	6.25	0.0897	61.29
Ascorbic acid	100	0.0053	97.70
	50	0.0377	83.74
	25	0.0670	71.08
	12.5	0.0990	57.27
	6.25	0.146	36.98

For Halliwell and Gutteridge [15], antioxidants are molecules that react with various reactive species at varying rates. Interestingly, at intermediate concentrations (25 and 12.5 ppm), ravenelin exhibited an antioxidant capacity statistically similar to that of ascorbic acid (*p-value* > 0.05). However, at the lowest concentration tested (6.25 ppm), ravenelin showed a significantly higher antioxidant capacity than ascorbic acid (*p-value* < 0.0001). Therefore, while the activity of ascorbic acid decreases with the reduction of its concentration, the activity of ravenelin remains within the same percentage range (approximately around 60%).

The results indicate that ravenelin shows promising potential as an antioxidant compound once, in an aqueous solution and at lower concentrations, this xanthone exhibits an antioxidant capacity greater than 50%, providing the first insights of its antioxidant action, and potential to be used in pharmaceutical, food and cosmetic industries.

3.2. Intramolecular H-bonds and infrared spectra analysis

Fig. 4 shows the minimal energy structures obtained for RVL and RVLB molecules. As one can observe, all OH groups form intramolecular OH···O structures, which presents the first indications regarding the position from which the hydrogen atom will be abstracted. According to theory, this abstraction must occur from the weakest hydrogen-bonded site [38], which is assigned by the highest H-bond length. In the particular case of RVL and RVLB, these distances (2.20 and 2.17 Å) correspond respectively to the **4-OH** and **2-OH** positions. Furthermore, according

Table 2
Infrared mode assignment for ravenelin and ravenelin B. The theoretical results were calculated using the theory level B3LYP/6-311++G(2*d*, 2*p*) within the IEF-PCM model, wavenumber values in cm^{-1}.

Ravenelin			Assignment	Ravenelin B			Assignment
Gas	Benzene	Water		Gas	Benzene	Water	
768	758	719	O−H out-of-plane bending (HB)	762	759	756	O−H out-of-plane bending (HB)
1077	1069	1039	C−O−C symmetric stretching	797	786	793	O−H out-of-plane bending (HB)
1229	1220	1199	C−O−C asymmetric stretching	1081	1086	1077	C−O−C symmetric stretching
1253	1244	1226	C−O−C asymmetric stretching	1216	1221	1220	C−O−C asymmetric stretching
1305	1305	1272	O−H in-plane deformation	1266	1263	1258	C−O−C asymmetric stretching
1337	1336	1313	O−H in-plane deformation	1353	1349	1340	O−H in-plane deformation
1405	1404	1382	CH_3 deformation		1399	1399	CH_3 deformation
1501	1497	1484	C=C stretching	1472	1469	1465	C=C stretching
1541	1535	1519	C=C stretching	1509	1504	1497	C=C stretching
1609	1599	1578	C=O stretching	1629	1625	1618	C=O stretching
1633	1630	1601	C=O stretching	1668	1664	1662	C=O stretching
1661	1657	1645	C=O stretching	1697	1698	1696	C=O stretching
3367	3349	3336	O−H stretching	3356	3352	3339	O−H stretching
3455	3436	3398	O−H stretching	3407	3399	3385	O−H stretching
3815	3804	3770	O−H stretching	3786	3782	3778	O−H stretching

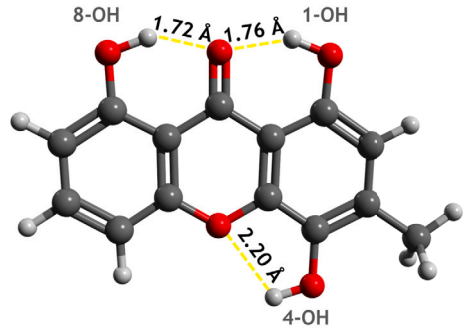

(a) RVL

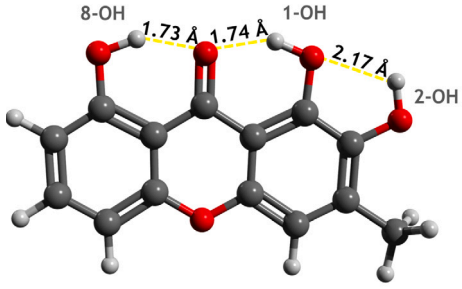

(b) RVLB

Fig. 4. The B3LYP/6-311++G(2*d*, 2*p*) optimized geometries of ravenelin and ravenelin B in gas phase.

to the results shown in **Table S3**, the solvent seems to facilitate the removal of hydrogen in these two hydroxyl groups. From gas to the aqueous environment, for instance, the OH···O bond length increases to 2.21 Å for the **4-OH** in ravenelin, as well to 2.19 Å for **2-OH** in ravenelin B, indicating that these H-bonds are even weaker in solvent.

The compounds studied in this work, Ravenalin (RVL) and Ravenalin B (RVLB), are positional isomers differing from each other solely by the location of the OH hydroxyl group (see Fig. 1) in relation to the xanthone ring. For the compound RVL, the hydroxyl is located at position 4 of the A ring moiety of the xanthone, and in the compound RVLB it occupies position 2 on this ring [39].

Such molecular configurations influence the positions and sizes of the intramolecular hydrogen bonds (HB) obtained in this work (see Fig. 4) and which in turn can be studied via IR spectrum (**Figure S1**) in order to determine the molecular conformations of the groups involved and adjacent groups. For example, it is well known that the stretching frequency of the carbonyl group (C=O) decreases by c. 40-60 cm^{-1} [40] regardless of whether the hydrogen bond is inter or intramolecular. On the other hand, a deformation in the xanthone ring can promote an increase in the stretching frequency of the carbonyl, the greater the deformation, the greater the increase in frequency [40].

It is also worth noting that hydroxyl has a stretching mode whose precise position depends on the magnitude of the hydrogen bond in which the group is involved [41], such an intramolecular bridge can result in a band in the region 3400-3600 cm^{-1} that is narrow and indifferent to the solvent [42]. Next, we will discuss how such effects influence the IR modes of RVL and RVLB compounds. For this purpose, we will use theoretical spectra obtained via DFT in three different environments, namely, gas phase, benzene (nonpolar), and water (polar), and also experimental results obtained using the FT-IR ATR setup.

It is possible to split the spectra based on the characteristic vibrational modes of two molecular groups that give shape to the compounds: (*i*) xanthone ring, (*ii*) hydroxyl. First, we will analyze the results for the compound RVL (OH in position 4 of ring A) whose characteristic modes are presented in Table 2 for the experimental spectra, gas phase and in the solvents benzene and water. The indicated assignments are in reasonable agreement with those published in previous experimental and theoretical works [43,44,48,49] that analyze the xanthone compound, specifically molecular group (*i*), while the addition of group (*ii*) produces some deviations in the original xanthone ring's frequencies. For example, the mode related to the stretching of the C=C double bond of the xanthone ring adjacent to those sites where group (*ii*) is bound undergo a reduction in the usual frequency of this vibration [44] which is around 1500 cm^{-1} in the RVL compound always as a very intense doublet [45] for all environments studied, with a more pronounced deviation in the solvent is water, where υ(C=C) appears at 1484 cm^{-1} and 1519 cm^{-1} (at 1498 cm^{-1} and 1506 cm^{-1} in experimental spectrum) a deviation of ~20 cm^{-1} in relation to the gas phase. Regarding the intensity of the first mode, it is possible to observe that in water (also in experimental spectra) it is relatively more intense compared to the carbonyl C=O stretching mode in the same solvent, which does not occur in the gas phase and in benzene (nonpolar). This suggests that in aqueous solution the vibration of the double bond of the xanthone ring becomes more vigorous than that of the carbonyl likely due to the polarity effects of the solvent. In what follows we will check the impact of this on the antioxidant action of RVL.

Changes are also observed in two important characteristic modes of RVL, namely, C−O−C stretching and C=O stretching of the carbonyl, both groups located at B ring of the xanthone. We start with the υ(C−O−C) mode, it occurs in two regions, the first referring to the symmetric stretching around 1050 cm^{-1} which in water appears at 1039 cm^{-1} (1062 cm^{-1} experimental) and which presents a devia-

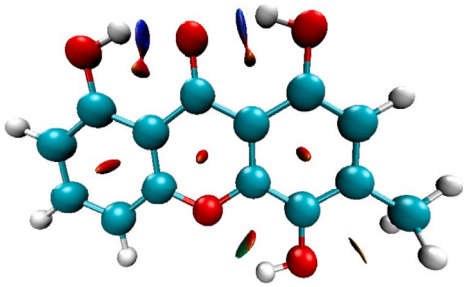

(a) RVL

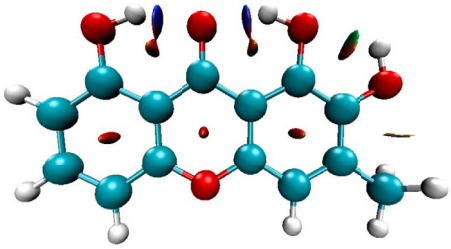

(b) RVLB

Fig. 5. Reduced gradients isosurfaces for RLV and RLVB. Atoms in light blue, white, and red denote carbon, hydrogen, and oxygen, respectively.

tion of 38 cm^{-1} compared to the gas phase (1077 cm^{-1}) and appears to have a shoulder at c. 1068 cm^{-1}, which is not observed in other environments. These effects are possibly caused by the polarity of the aqueous environment but mainly by the participation of this group in one of the intramolecular HB, 4−OH···O, whose length, 2.20 Å, is the longest among the three intramolecular bridges present in the RVL (see Fig. 4). The combination of intramolecular HB and solvent polarity stabilizes the molecule resulting in the doubling of υ(C=C) [46], remembering that these modes suffer deviations due to polarity, but their intensities remain almost unchanged in any environment studied.

This situation suggests a more planar conformation of the RVL, making the molecule slightly more stable, that is, the C−O−C group tends to assume a *trans* configuration while the *cis* one tends to be inhibited (steric effect) [46]. The second region, the asymmetric υ(C−O−C), located around 1200 cm^{-1} is where we find, in water, a doublet, 1199 cm^{-1} and 1226 cm^{-1}, and which shows a deviation of ~30 cm^{-1} in relation to the gas phase. Here the combined role of PH and solvent polarity also produces an inversion of the doublet's intensity, making the 1199 cm^{-1} peak more intense than its companion 1226 cm^{-1}, something that is not observed in any other tested environment. As seen, the υ(C−O−C) stretching mode provides valuable information about the interaction of RVL with the solvent but also about the influence of PH 4−OH···O on the conformational stability of the molecule.

3.3. Energetic H-bond definition using AIM and NCI analysis

To reinforce our previous analysis, we employed the AIM to characterize the topological parameters $\rho(r)$ and λ_2. This approach is useful for following trends in the strength of intramolecular H-bonds. Considering that $\lambda_2 < 0$ and $\lambda_2 > 0$ values imply binding and repulsive interaction, respectively, we notice that the intermolecular H-bonds formed in **1-OH** and **8-OH** sites of both RVL and RVLB are relatively strong. Fig. 5 depicts the calculated reduced gradients isosurfaces (RDG) for both Ravenelin and Ravenelin B.

Starting the discussion, we noticed that the RDG isosurfaces are similar in gas phase and water solvent. These resemblances reflect the slight differences in $\rho(r)$ and the H-bond binding energies in different dielectric constants. For instance, in the case of the RLV, the found value for H-bond binding in the **1-OH** site is -35.31 kJ/mol, and considering the water solvent environment, the value increases reading -37.45 kJ/mol.

Table 3
Calculated topological parameters $\rho(r)$ and λ_2 and H-bond binding energy (kJ/mol) for both RVL and RVLB at B3LYP/6-311++G($2d, 2p$).

		RVL		RVLB	
Environment	Parameter	1-OH	8-OH	1-OH	8-OH
Gas	H-bond B.E.*	-35.31	-39.58	-36.57	-40.17
	$\rho(r)$	0.041	0.046	0.043	0.046
	λ_2	-0.041	-0.046	-0.043	-0.046
Water	H-bond B.E.*	-37.45	-38.24	-37.40	-39.50
	$\rho(r)$	0.043	0.044	0.043	0.046
	λ_2	-0.043	-0.044	-0.043	-0.046

* Calculated by H-bond B.E $\approx -223.08 \times \rho(r) + 0.7423$ [36].

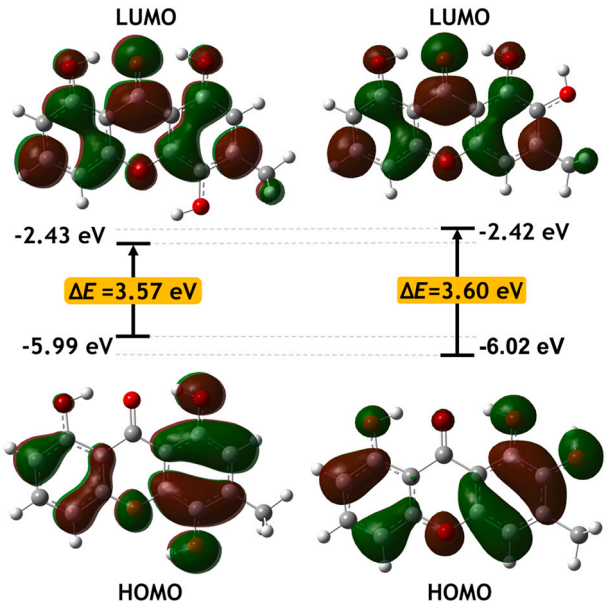

Fig. 6. The frontier molecular orbitals of ravenelin (left) and ravenelin B (right) molecules calculated using the B3LYP/6-311++G(*2d,2p*) method at gas phase.

Same for **8-OH**, which in turn, the H-bond is strongest with binding energies values around -37.0 kJ/mol. These values are in agreement with the previously calculated for conventional intramolecular H-bonds [47], see Table 3.

Moreover, the RDG isosurfaces in blue color depicted in Fig. 5 suggest relatively strong interactions. In this sense, these findings ensure that the hydrogen abstraction does not take place in **1-OH** and **8-OH** positions for both RLV and RLVB. On the contrary, RDG isosurfaces (see Fig. 5) suggest that the interactions formed between 4-OH in RLV and **2-OH** in RLVB and their respective neighboring oxygen atoms are weak/repulsive. In this point, it is worth commenting that a bond path denotes a bonded interaction, in this sense, we noticed that bond paths were not formed between these latter sites (see **Fig S2**). These findings reinforce that the hydrogen abstraction takes place at **4-OH** and **2-OH** positions in RLV and RLVB, respectively.

3.4. Frontier orbitals and intramolecular charge transfer

The next stage is to determine the connections between the hydrogen transfer procedure to the molecular electronic structure. From Fig. 6, one can analyze the topology of the frontier molecular eigenstates of both ravenelin molecules. It is assumed that the hydrogen atom will be removed from the region where the HOMO state has the highest localization [54]. Additionally, the OH group subjected to a free radical attack shows a lower contribution from the LUMO state compared to the HOMO state. According to Fig. 6, these sites correspond to the **4-OH** and **2-OH** respectively in RVL and RVLB.

Table 4
Bond dissociation enthalpy (BDE) and the variation of BDE of xanthones with the reference of ascorbic acid (ΔBDE) values with 6-311++G(2p, 2d) level of theory. The simulations in the gas phase, in apolar and polar environments with the IEF-PCM method.

		BDE (kJ/mol)			ΔBDE (kJ/mol)		
Comp.	Bonds	Gas	Benzene	Water	Gas	Benzene	Water
RVL	1-OH	379	365	351	61	49	37
	4-OH	322	317	312	4	1	-1
	8-OH	411	399	383	93	83	69
RVLB	1-OH	357	347	334	39	31	21
	2-OH	342	334	323	24	18	10
	8-OH	404	393	378	86	77	65
Ascorbic acid		318	316	313			

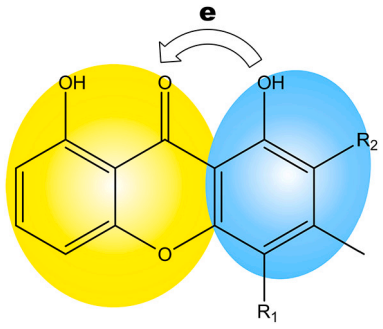

Fig. 7. A schedule for the intramolecular charge transfer procedure obtained for ravenelin and ravenelin B molecules.

Moreover, the topology of the HOMO and LUMO states suggests the occurrence of an intramolecular charge transfer (ICT) process involving the flow of charges from a donor (D) to an acceptor (A) site within the molecules. However, a simple analysis of the molecular orbital topology is insufficient to fully characterize an ICT process once other excitations can also balance the charge redistribution. To gain a better understanding of this effect, one can examine the electronic distribution of the Franck-Condon vertical state and analyze the molecular dipole moment (see **Table S4**) [50].

For RVLB as the first study case, one obtains respective ground state and Franck-Condon dipole moments of $\mu_{GS} = 2.75$ D and $\mu_{FC} = 5.30$ D, clearly indicating a strong charge redistribution. After analyzing the q_{GS} and q_{FC} Mulliken charges, one obtains values of -0.106e and 0.067e in the blue surface shown in Fig. 7. This result ($q_{FC} - q_{GS} > 0$) indicates that this region loses electronic density. In solvent, the ICT process is enhanced independent of the environment polarity. For instance, in water solvent, one obtains μ_{GS} and μ_{FC} values of 3.94 and 7.34 D, confirming the ICT effect.

Although there are other successful strategies to describe partial atomic charges, a simple analysis of the Mullikan charges obtained using the 6-311++G(d, p) basis set has provided consistent results in comparison to other methods [51]. This feature gives more reliability to the discussion.

3.5. Spin density analysis

Fig. 8 shows the spin density distribution (SDD) and the spin population calculated for each RVLB radical. According to theory, the stability of a radical can be characterized by the spin density distribution. A more delocalized spin density, a lower spin population on O-atom. As a consequence, the more stable the radical, and smaller the BDE [52,53]. However, in both xanthones, one observes a contradiction. For RVLB, spin density appears to be more delocalized for the **1-OH** (0.237) radical than those located on **8-OH** (0.296) and **2-OH** (0.344). This prediction is in evident contradiction to the results shown for the BDE values in Table 4 which indicates that **2-OH** < **1-OH** < **8-OH** is growing order.

For the RVL, the spin density distribution and spin density population on each atom are shown in **Fig. S4**, the results are similar. Again, one obtains greater delocalization on the **1-OH** (0.276) radical than **8-OH** (0.309) and **4-OH** (0.330), which goes against the BDE growth order, **4-OH** < **1-OH** < **8-OH**. As a consequence, the analysis of the spin density population can not be applied at least for these xanthones and the discussion of radical stability must be held in terms of dissociation energies. This feature is not a particularity of xanthone molecules. Similar conditions were found in Trolox, which is a well-established and studied antioxidant compound [53].

3.6. HAT mechanism

A graphical analysis based on the topologies of the frontiers orbitals as well as spin densities does not provide a comparison between the antioxidant performances of two chromophores. This goal is achieved by experimental assays or theoretical analysis of molecular enthalpies. We shall discuss this last subject now, and with this goal, Table 4 presents the BDE parameters that define the HAT mechanism. From Fig. 4 both molecules present hydroxyl and methyl groups that can loss a hydrogen in abstraction process. However, we focus only on the hydroxyl groups, once Tiwari and Mishra have previously shown [37] that this one is more susceptible to a radical attack.

Starting from RVL and based on the gas phase results, the **4-OH** radical exhibits the lowest enthalpy of dissociation (322 kJ/mol), which is consistent with the analysis of molecular orbitals and spin densities. Comparing this value to that obtained for the isolated ascorbic acid molecule as reference ($\Delta BDE = BDE_{molecule} - BDE_{reference}$), we observe a positive energetic variation of 4 kJ/mol indicating that at gas-phase, RVL has worse performance in comparison to AA.

Posteriously, the contributions of the solvent are systematically accounted for by using the IEF-PCM to simulate benzene, an apolar and aprotic solvent, as well as water. The behavior realized is curious and reveals a dependence on the solvent polarity. For instance, in benzene, the **4-OH** RVL radical predicts a dissociation energy of 317 kJ/mol, which is a reduction regarding its gas-phase value, and indicates that the solvent facilitates the process of hydrogen transfer. Besides, the ΔBDE is down to only 1 kJ/mol, giving a signal that the solvent trends to improve the antioxidant performance of RVL in comparison to AA.

The role of the solvent polarity becomes more evident in aqueous environment. The results of quantum mechanics indicate a dissociation enthalpy of 312 kJ/mol for **4-OH** radical, resulting in a ΔBDE of -1 kJ/mol regarding the reference. The negative signal means that the energy necessary for the hydrogen transfer becomes lower than that estimated for ascorbic acid. However, although this is a slight difference, it moves in the same direction as the experimental results shown in Table 1. One observes that RVL shows an antioxidant efficiency (61%) much greater than ascorbic acid (37%) at the lowest concentration (6.25 ppm), which is the situation simulated by PCM.

Regarding RVLB, the DFT results are not as encouraging as those obtained for RVL, but indicate what might be an interesting antiox-

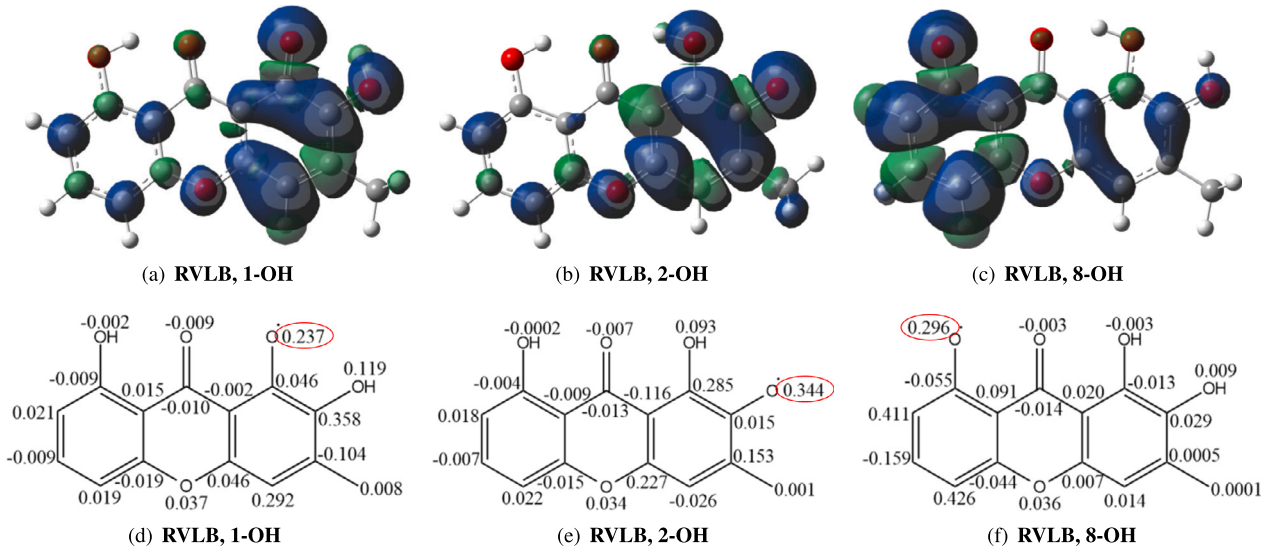

Fig. 8. The plot of spin density distribution (a-c) and numerical values of the spin density population (d-f) of unrestricted B3LYP/6-311++G(2d, 2p) total atomic spin densities distributions for radical molecules of ravenelin B in vacuum. While the green color represents down spin, the blue one designates up spin density, which dominates the surfaces.

Table 5
Proton Affinities (PA) and Electron Transfer Enthalpies (ETE) values with B3LYP/6-311++G(2p, 2d) level of theory. The simulations in the gas phase, in apolar and polar environments with the IEF-PCM method.

	PA (kJ/mol)			ETE (kJ/mol)			SPLET (kJ/mol)		
Comp.	Gas	Benzene	Water	Gas	Benzene	Water	Gas	Benzene	Water
RVL									
1-OH	1431	429	149	267	347	326	1698	776	474
4-OH	1408	409	135	233	319	300	1641	727	436
8-OH	1421	417	142	308	393	364	1730	810	506
RVLB									
1-OH	1392	395	122	283	363	336	1675	758	458
2-OH	1426	424	143	235	321	304	1661	745	447
8-OH	1423	421	143	300	383	359	1723	803	502
Ascorbic acid	1315	319	58	322	407	379	1637	726	437

idant behavior. For example, under gas phase conditions, the **2-OH** RVLB radical is predominant, confirming the analysis carried out for the HOMO/LUMO, spin densities, and the infrared spectra interpretation. However, the predicted value for the **2-OH** radical is 342 kJ/mol, which is approximately 20 kJ/mol higher than the estimated value for RVL. On the other hand, it exhibits a positive variation in bond dissociation energy of 24 kJ/mol compared to the reference AA molecule. Once again, the solvent improves this behavior. In the presence of benzene and water solvents, one obtains ΔBDE values of 18 and 10 kJ/mol, respectively. Again, the increase of the solvent polarity improves the antioxidant behavior of the studied molecule.

3.7. SET-PT mechanism

As discussed earlier, the SET-PT mechanism involves a sequential process in which electron transfer occurs first, followed by proton shifting. These stages are represented by the IP and PDE parameters, as shown in **Table S5**. Upon initial analysis, it becomes evident that this specific hydrogen removal mechanism does not take place either in the gas phase or in a solvent. For example, the DFT results for IP, which is the first stage of the SET-PT mechanism, are estimated as 717 and 717 kJ/mol for RVL and RVLB, respectively. These values are significantly higher than those reported for HAT, indicating that the SET-PT mechanism is unlikely to occur under gas phase conditions. The same conclusions can be drawn for solvent environments, such as benzene and water in the case of RVL. In these two solvents, ionization potentials of 614 and 445 kJ/mol are obtained, respectively. Although the solvent reduces the activation energy of the chemical reaction, the values obtained for the first stage of the SET-PT mechanism remain higher than those reported for HAT in both solvents.

Although the SET-PT process is not energetically viable, it is interesting to realize its total energetic demand, given by the sum of IP plus PDE enthalpies. According to **Table S5**, for RVL molecules in both gas and water environments, the **4-OH** is the prevalent radical. On the other hand, **2-OH** is the ordinary one. Consequently, again one obtains agreement with the HOMO-LUMO and spin density analysis.

3.8. SPLET mechanism

The last hydrogen transfer mechanism (SPLET) also occurs following sequential stages. In this case, a proton loss happens first, followed by an electron transfer. Table 5 presents the PA and ETE parameters, which describe this mechanism. According to the B3LYP/6-311++G(2d, 2p) results, this mechanism is not allowed for both compounds in the gas phase. The RVL molecule, for instance, presents PA values varying from 1408 to 1431 kJ/mol, which is much higher than those reported for the HAT mechanism. Once the same conclusion is observed for RVLB, one obtains that the HAT mechanism dominates the hydrogen transfer procedure for isolated RVL and RVLB compounds.

However, according to the results, the configuration above changes when the polarity of the solvent increases. For benzene, which is a non-polar and aprotic solvent, all PA values calculated for both RVL and

RVLB remain higher than those estimated for BDE values shown in Table 4. Consequently, the HAT mechanism prevails in non-polar or less polar solvents like benzene.

On the other hand, for polar environments such as water, the behavior is quite different. In this case, the calculated PA enthalpies become lower than those obtained for BDE in aqueous solvent. For instance, one obtains values varying from 135 to 149 kJ/mol for the proton affinity of RVL molecules, which are much lower values than those obtained for the HAT and SET-PT mechanisms in water. Moreover, similar conclusions can be made for RVLB molecule. These findings indicate that the solvent can change the hydrogen transfer mechanism from gas to liquid phase, presenting great dependence regarding polarity of the medium, which must be carefully observed if one desires to model and understand the antioxidant apparatus. Similar conclusions as organic dyes like isoflavones [6], coumarins [7], and other systems [55–59].

Table 5 also shows the sum of PA and PDE parameters for all molecular radicals investigated. For both gas and solvent environments, the DFT analysis indicates that the **2-OH** radical is preferred for RVL, whereas the **4-OH** structure prevails in the antioxidant process played by RVLB. Again, these results are in consonance with the orbital and spin density. Table 5 also shows the PA and PDE sum for all molecular radicals investigated. For both gas and solvent environments, the DFT analysis indicates that the **2-OH** radical is preferred for RVL, whereas the **4-OH** structure prevails in the antioxidant process played by RVLB.

Again, these results align with the orbital and spin density scanning, as well as with the experimental prediction. Notably, it is possible to build an antioxidant scale in which RVL > ascorbic acid > RVLB in water solvent. For instance, according to the results shown in Table 5, the total dissociation energy need for hydrogen abstraction in the SPLET mechanism is 436 kJ/mol for RVL in the **4-OH** position, which is clearly lower than the values of 437 and 447 kJ/mol, respectively obtained for ascorbic acid and RVLB at the **2-OH** position in water solution.

Finally, recent reports indicate that the antioxidant behavior of RVL and RVLB can be greater than that estimated by the current theoretical methodology. Besides the three hydrogen abstraction routs discussed above, it is possible to occur the Sequential Proton Loss - Hydrogen Atom Transfer (SPLHAT) [60–64] and Sequential Triple Proton Loss Double Electron Transfer (StPLdET) [65,66] mechanisms. In these procedures, the hydrogen transfer is assisted by additional abstractions of proton and electron. For instance, it has been reported that the bond dissipation energy necessary to remove the hydrogen atom in the SPLHAT mechanism might be ~33 kJ/mol lower than that found in a single HAT occurrence [66].

4. Conclusions

Based on the framework of the Density Functional Theory and experimental techniques, it is carried out a systematic discussion of the antioxidant behavior of ravenelin and ravenelin B molecules, two compounds recently extracted from the endophytic *Exserohilum rostratum* fungus. Ravenelin and ravenelin B are position isomers. However, besides their structural similarities, our experimental and quantum chemical assays show that they present different antioxidant behaviors in comparison to ascorbic acid, which is an industrial antioxidant reference. While ravenelin B exhibits slightly lower antioxidant action than that exhibited by the standard, both theoretical and experimental approximations indicate that ravenelin shows superior behavior to the reference compound. Consequently, it is determined scale of antioxidant behavior, ravenelin > ascorbic acid > ravenelin B

The analysis of the thermochemistry, molecular, and electronic structures of the chromophores indicates that the polarity of the solvent and the intramolecular hydrogen bond formation plays a fundamental role in the hydrogen transfer procedure. The vibrational analysis of the OH stretching modes and molecular enthalpies shows that the hydrogen abstraction takes place at the molecular site where the hydrogen bond is weakest. Moreover, the calculations of electronic structure reveal that the solvent and its polarity are active actors in the process of hydrogen abstraction. Under gaseous conditions, the dominant antioxidant mechanism is the Hydrogen Atom Transfer, which also prevails in non-polar solvents like benzene. However, in polar environments the antioxidant route changes to the Sequential Proton Loss - Electron Transfer. Besides the understanding of how the antioxidant mechanism occurs for ravenelin B, the results indicate that these chromophores are promising to the pharmacological industry.

CRediT authorship contribution statement

N.S.S. dos Santos: Methodology, Investigation, Formal analysis, Data curation. **H.B. Barbieri:** Methodology, Investigation, Formal analysis, Data curation. **M. Pinheiro:** Methodology, Investigation, Formal analysis, Data curation. **T.P. Fill:** Writing – review & editing. **M.H. Queiroz:** Methodology, Investigation, Formal analysis, Data curation. **J. Pina:** Methodology, Formal analysis, Data curation. **E. Belo:** Investigation, Formal analysis, Data curation. **H.C. Georg:** Writing – review & editing, Writing – original draft. **A.R. da Cunha:** Writing – original draft. **P.S.B. Marinho:** Methodology, Investigation, Formal analysis, Data curation. **A.M.R. Marinho:** Writing – original draft, Methodology, Investigation, Formal analysis, Data curation. **K. Coutinho:** Writing – original draft, Methodology, Investigation, Data curation. **S. Canuto:** Writing – review & editing, Writing – original draft. **R. Gester:** Writing – review & editing, Writing – original draft.

Declaration of competing interest

The authors declare that they have no known competing financial interests or personal relationships that could have appeared to influence the work reported in this paper.

Data availability

No data was used for the research described in the article.

Acknowledgements

This study is financed in part by the Coordenação de Aperfeiçoamento de Pessoal de Nível Superior - Brasil (CAPES), Conselho Nacional de Desenvolvimento Científico e Tecnológico (CNPq), Fundação de Amparo à Pesquisa do Estado de São Paulo (FAPESP). H.B.B. thanks to FAPESP, 2021/08947-3. M.P. thanks to CNPq, 142600/2021-0. K.C. acknowledges to the National Institute of Science and Technology Complex Fluids (INCT-FCx), financed by CNPq (141260/2017-3) and FAPESP (2014/50983-3 and 2018/20162-9). This research was done with the computational support of Laboratório Multiusuário de Computação de Alto Desempenho (LaMCAD/UFG).

Appendix A. Supplementary material

Supplementary material related to this article can be found online at https://doi.org/10.1016/j.molliq.2024.125045.

References

[1] I.Z. Sadiq, Free radicals and oxidative stress: signaling mechanisms, redox basis for human diseases, and cell cycle regulation, Curr. Mol. Med. 23 (2023) 13–35, https://doi.org/10.2174/1566524022666211222161637.

[2] D. Krishnaiah, R. Sarbatly, R. Nithyanandam, A review of the antioxidant potential of medicinal plant species, Food Bioprod. Process. 89 (2011) 217–233, https://doi.org/10.1016/j.fbp.2010.04.008.

[3] S. Mahmoudi, M.M. Dehkordi, M.H. Asgarshamsi, Density functional theory studies of the antioxidants-a review, J. Mol. Model. 27 (2021) 271, https://doi.org/10.1007/s00894-021-04891-1.

[4] P.C. Nam, M.V. Bay, Q.V. Vo, A. Mechler, N.M. Thong, Tautomerism and antioxidant power of sulfur/-benzo[h]quinoline: DFT and molecular docking studies, J. Mol. Liq. 363 (2022) 119908, https://doi.org/10.1016/j.molliq.2022.119908.

[5] S. Molaei, A.D. Tehrani, H. Shamlouei, Antioxidant activates of new carbohydrate based gallate derivatives: a DFT study, J. Mol. Liq. 377 (2023) 121506, https://doi.org/10.1016/j.molliq.2023.121506.

[6] S. Fonseca, N.S.S. dos Santos, A. Torres, M. Siqueira, A. da Cunha, V. Manzoni, P.F. Provasi, R. Gester, S. Canuto, The role of the solvent and intramolecular hydrogen bonds in the antioxidative mechanism of prenylisoflavone from leaves of Vatairea guianensis, J. Phys. Chem. A 127 (2023) 10807, https://doi.org/10.1021/acs.jpca.3c05725.

[7] G. Wang, Y. Liu, L. Zhang, L. An, R. Chen, Y. Liu, Q. Luo, Y. Li, H. Wang, Y. Xue, Computational study on the antioxidant property of coumarin-fused coumarins, Food Chem. 304 (2020) 125446, https://doi.org/10.1016/j.foodchem.2019.125446.

[8] J.R.S. Pina, et al., Antiprotozoal and antibacterial activity of ravenelin, a xanthone isolated from the endophytic fungus exserohilum rostratum, Molecules 26 (2021) 3339, https://doi.org/10.3390/molecules26113339.

[9] G.J. Papariello, M.A.M. Janish, Diphenylpicrylhydrazyl as an organic analytical reagent in the spectrophotometric analysis of phenols, Anal. Chem. 38 (1966) 211, https://doi.org/10.1021/ac60234a016.

[10] B.N. Ames, M.K. Shigenaga, T.M. Hagen, Oxidants, antioxidants, and the degenerative diseases of aging, Proc. Natl. Acad. Sci. 90 (1993) 7915, https://doi.org/10.1073/pnas.90.17.7915.

[11] O. Arrigoni, M.C. De Tullio, Ascorbic acid: much more than just an antioxidant, Biochim. Biophys. Acta G, Gen. Subj. 1569 (2002) 1, https://doi.org/10.1016/S0304-4165(01)00235-5.

[12] D. Njus, P.M. Kelley, Y.J. Tu, H.B. Schlegel, Ascorbic acid: the chemistry underlying its antioxidant properties, Free Radic. Biol. Med. 159 (2020) 3, https://doi.org/10.1016/j.freeradbiomed.2020.07.013.

[13] K. Mishra, H. Ojha, N.K. Chaudhury, Estimation of antiradical properties of antioxidants using DPPH assay: a critical review and results, Food Chem. 130 (2012) 1036, https://doi.org/10.1016/j.foodchem.2011.07.127.

[14] L.Y. Ho, et al., Comparison of physicochemical properties and aqueous solubility of xanthone prepared via oil-in-water emulsion and complex coacervation techniques, Int. J. Food Prop. 21 (2018) 784, https://doi.org/10.1080/10942912.2018.1446022.

[15] B. Halliwell, J.M.C. Gutteridge, Free Radicals in Biology and Medicine, Oxford University Press, USA, 2015.

[16] A. Urbaniak, J. Kujawski, K. Czaja, M. Szelag, Antioxidant properties of several caffeic acid derivatives: a theoretical study, C. R., Chim. 20 (2017) 1072–1082, https://doi.org/10.1016/j.crci.2017.08.003.

[17] A.D. Becke, Density-functional thermochemistry. III. The role of exact exchange, J. Chem. Phys. 98 (1993) 5648–5652, https://doi.org/10.1063/1.464913.

[18] C. Lee, W. Yang, R.G. Parr, Development of the Colle-Salvetti correlation-energy formula into a functional of the electron density, Phys. Rev. B 37 (1988) 785, https://doi.org/10.1103/physrevb.37.785.

[19] S.H. Vosko, L. Wilk, M. Nusair, Accurate spin-dependent electron liquid correlation energies for local spin density calculations: a critical analysis, Can. J. Phys. 58 (1980) 1200, https://doi.org/10.1139/p80-159.

[20] T. Clark, J. Chandrasekhar, G.W. Spitznagel, P.V.R. Schleyer, Efficient diffuse function-augmented basis sets for anion calculations. III. The 3-21+G basis set for first-row elements, Li-F, J. Comput. Chem. 4 (1983) 294, https://doi.org/10.1002/jcc.540040303.

[21] R. Krishnan, J.S. Binkley, R. Seeger, J.A. Pople, Self-consistent molecular orbital methods. XX. A basis set for correlated wave functions, J. Chem. Phys. 72 (1980) 650, https://doi.org/10.1063/1.438955.

[22] S. Miertuš, E. Scrocco, J. Tomasi, Electrostatic interaction of a solute with a continuum. A direct utilization of ab initio molecular potentials for the prevision of solvent effects, Chem. Phys. 55 (1987) 117–129, https://doi.org/10.1016/0301-0104(81)85090-2.

[23] M.J. Frisch, et al., Gaussian 16, Revision C.01, Gaussian Inc., Wallingford CT, 2016.

[24] A. Urbaniak, M. Szela, M. Molski, Theoretical investigation of stereochemistry and solvent influenceon antioxidant activity of ferulic acid, Comput. Theor. Chem. 2012 (2013) 33–40, https://doi.org/10.1016/j.comptc.2013.02.018.

[25] R.F.W. Bader, Atoms in Molecules, Oxford University Press, Oxford, 1990.

[26] R.F.W. Bader, Acc. Chem. Res. 18 (1985) 9–15, https://doi.org/10.1021/ar00109a003.

[27] R.F.W. Bader, A quantum theory of molecular structure and its applications, Chem. Rev. 91 (1991) 893–928, https://doi.org/10.1021/cr00005a013.

[28] E.R. Johnson, S. Keinan, P. Mori-Sánchez, J. Contreras-García, A.J. Cohen, W. Yang, Revealing noncovalent interactions, J. Am. Chem. Soc. 132 (2010) 6498–6506, https://doi.org/10.1021/ja100936w.

[29] J. Contreras-García, E.R. Johnson, S. Keinan, R. Chaudret, J.-P. Piquemal, D.N. Beratan, W. Yang, NCIPLOT: a program for plotting noncovalent interaction regions, J. Chem. Theory Comput. 7 (2011) 625–632, https://doi.org/10.1021/ct100641a.

[30] T. Lu, F. Chen, Multiwfn: a multifunctional wavefunction analyzer, J. Comput. Chem. 33 (2012) 580–592, https://doi.org/10.1002/jcc.22885.

[31] W. Humphrey, A. Dalke, K. Schulten, VMD: visual molecular dynamics, J. Mol. Graph. 14 (1996) 33–38, https://doi.org/10.1016/0263-7855(96)00018-5.

[32] V. Silber, C. Gourlaouen, R. Ruppert, Keto–enol equilibrium: stable tautomers of ortho-, meta-, and para-hydroquinones in large aromatics, RSC Adv. 14 (2024) 11969, https://doi.org/10.1039/D4RA02202E.

[33] T. Lukmanov, S.P. Ivanov, E.M. Khamitov, S.L. Khursan, Relative stability of keto-enol tautomers in 5, 6-substituted uracils: ab initio, DFT and PCM study, Comput. Theor. Chem. 1023 (2013) 38, https://doi.org/10.1016/j.comptc.2013.09.005.

[34] C.S. Cucinotta, A. Ruini, A. Catellani, A. Stirling, Ab initio molecular dynamics study of the Keto–Enol tautomerism of Acetone in solution, ChemPhysChem 7 (2006) 1229, https://doi.org/10.1002/cphc.200600007.

[35] E.A. Abourashed, Thin-layer densitometry as an alternative tool in the quantitative evaluation of the free radical scavenging activity of natural antioxidants, Z. Naturforsch. B 60 (2005), https://doi.org/10.1515/znb-2005-1116.

[36] S. Emamian, T. Lu, H. Kruse, H. Emamian, Exploring nature and predicting strength of hydrogen bonds: a correlation analysis between atoms-in-molecules descriptors, binding energies, and energy components of symmetry-adapted perturbation theory, J. Comput. Chem. 40 (2019) 2868–2881, https://doi.org/10.1002/jcc.26068.

[37] M.K. Tiwari, P.C. Mishra, Scavenging of hydroxyl, methoxy, and nitrogen dioxide free radicals by some methylated isoflavones, J. Mol. Model. 24 (2018) 287, https://doi.org/10.1007/s00894-018-3805-6.

[38] S. Scheiner, Hydrogen Bonding: A Theoretical Perspective, first edition, Oxford University Press, New York, 1977, p. 375.

[39] T. Wezeman, S. Bräse, K.S. Masters, Xanthone dimers: a compound family which is both common and privileged, Natl. Prod. Rep. 32 (2015) 6–28, https://doi.org/10.1039/c4np00050a.

[40] G. Socrates, Infrared and Raman Characteristic Group Frequencies: Tables and Charts, Wiley, New York, 2004, p. 115.

[41] U. Liddel, Some simple hydrogen-bonding systems studied by infrared absorption, Ann. N.Y. Acad. Sci. 69 (1957) 70–83, https://doi.org/10.1111/j.1749-6632.1957.tb49650.x.

[42] G. Socrates, Infrared and Raman Characteristic Group Frequencies: Tables and Charts, Wiley, New York, 2004, p. 94.

[43] R.E. Connors, C.M. Fratini, Polarized IR and DFT study of the fundamental vibrations of xanthone, J. Mol. Struct. 553 (2000) 235–241, https://doi.org/10.1016/s0022-2860(00)00565-2.

[44] D. Cook, Infrared spectra of xanthone: Lewis acid complexes, Can. J. Chem. 41 (1963), https://doi.org/10.1139/v63-072.

[45] G. Socrates, Infrared and Raman Characteristic Group Frequencies: Tables and Charts, Wiley, New York, 2004, p. 161.

[46] G. Socrates, Infrared and Raman Characteristic Group Frequencies: Tables and Charts, Wiley, New York, 2004, p. 101.

[47] A.V. Afonin, A.V. Vashchenko, M.V. Sigalov, Estimating the energy of intramolecular hydrogen bonds from 1H NMR and QTAIM calculations, Org. Biomol. Chem. 14 (2016) 11199, https://doi.org/10.1039/C6OB01604A.

[48] H.K. Sinha, C. Lek, R.P. Steer, Vibrational spectra of xanthione and xanthone, J. Mol. Spectrosc. 169 (1995) 302–314, https://doi.org/10.1006/jmsp.1995.1025.

[49] R. Zwarich, O.S. Binbrek, Vibrational spectra of 9-xanthone, Spectrochim. Acta 41 (1985) 537–544, https://doi.org/10.1016/0584-8539(85)80041-6.

[50] R. Gester, M. Siqueira, A.R. Cunha, R.S. Araújo, P.F. Provasi, S. Canuto, Assessing the dipolar-octupolar NLO behavior of substituted thiosemicarbazone assemblies, Chem. Phys. Lett. 831 (2023) 140807, https://doi.org/10.1016/j.cplett.2023.140807.

[51] M. Uhliar, Atomic partial charge model in chemistry: chemical accuracy of theoretical approaches for diatomic molecules, Acta Chim. Slov. 17 (2024) 1–11, https://doi.org/10.2478/acs-2024-0001.

[52] C.J. Parkinson, P.M. Mayer, L. Radom, An assessment of theoretical procedures for the calculation of reliable radical stabilization energies, J. Chem. Soc. 11 (1999) 2305, https://doi.org/10.1039/A905476F.

[53] H. Boulebd, Comparative study of the radical scavenging behavior of ascorbic acid, BHT, BHA and Trolox: experimental and theoretical study, J. Mol. Struct. 1201 (2020) 127210, https://doi.org/10.1016/j.molstruc.2019.127210.

[54] Y. Xue, Y. Zheng, L. An, Y. Dou, Y. Liu, Density functional theory study of the structure–antioxidant activity of polyphenolic deoxybenzoins, Food Chem. 151 (2014) 198–206, https://doi.org/10.1016/j.foodchem.2013.11.064.

[55] M. Spiegel, K. Cel, Z. Sroka, The mechanistic insights into the role of pH and solvent on antiradical and prooxidant properties of polyphenols — nine compounds case study, Food Chem. 407 (2023) 134677, https://doi.org/10.1016/j.foodchem.2022.134677.

[56] M. Chen, Z. Li, G. Sun, S. Jin, X. Hao, C. Zhang, L. Liu, L. Zhang, H. Liu, Y. Xue, Theoretical study on the free radical scavenging potency and mechanism of natural coumestans: roles of substituent, noncovalent interaction and solvent, Phytochem. 207 (2023) 113580, https://doi.org/10.1016/j.phytochem.2022.113580.

[57] Y.Z. Zheng, G. Deng, R. Guo, Z.M. Fu, D.F. Chen, The influence of the H5⋯OC4 intramolecular hydrogen-bond (IHB) on the antioxidative activity of flavonoid, Phytochem. 160 (2019) 19, https://doi.org/10.1016/j.phytochem.2019.01.011.

[58] Y.Z. Zheng, D.F. Chen, G. Deng, R. Guo, Z.M. Fu, The antioxidative activity of piceatannol and its different derivatives: antioxidative mechanism analysis, Phytochem. 156 (2018) 184, https://doi.org/10.1016/j.phytochem.2018.10.004.

[59] Y.Z. Zheng, G. Deng, D.F. Chen, Q. Liang, R. Guo, Z.M. Fu, Theoretical studies on the antioxidant activity of pinobanksin and its ester derivatives: effects of the chain length and solvent, Food Chem. 240 (2018) 323, https://doi.org/10.1016/j.foodchem.2017.07.133.

[60] M. Musialik, R. Kuzmicz, T.S. Pawłowski, G. Litwinienko, Acidity of hydroxyl groups: an overlooked influence on antiradical properties of flavonoids, J. Org. Chem. 74 (2009) 2699, https://doi.org/10.1021/jo802716v.

[61] H. Boulebd, A. Mechler, T.H. Nguyen, Q.V. Vo, Insights on the kinetics and mechanisms of the peroxyl radical scavenging capacity of caftaric acid: the important role of the acid–base equilibrium, New J. Chem. 46 (2022) 7403, https://doi.org/10.1039/D2NJ00377E.

[62] R. Castañeda-Arriaga, T. Marino, N. Russo, J.R. Alvarez-Idaboy, A. Galano, Chalcogen effects on the primary antioxidant activity of chrysin and quercetin, New J. Chem. 44 (2020) 9073, https://doi.org/10.1039/D0NJ01795G.

[63] T.D. Ngoc, T.N. Le, T.V.A. Nguyen, A. Mechler, N.T. Hoa, N.L. Nam, Q.V. Vo, Mechanistic and kinetic studies of the radical scavenging activity of 5-O-Methylnorbergenin: theoretical and experimental insights, J. Phys. Chem. B 126 (2022) 702, https://doi.org/10.1021/acs.jpcb.1c09196.

[64] Y. Xue, L. Yunping, X. Yuxin, C. Cong, G. Wang, L. An, Y. Teng, M. Chen, L. Zhang, Antioxidant activity and mechanism of dihydrochalcone C-glycosides: effects of C-glycosylation and hydroxyl groups, Phytochem. 179 (2020) 112393, https://doi.org/10.1016/j.phytochem.2020.112393.

[65] A. Galano, J.R. Alvarez-Idaboy, Computational strategies for predicting free radical scavengers' protection against oxidative stress: where are we and what might follow?, Int. J. Quant. Chem. 118 (2018) e25665, https://doi.org/10.1002/qua.25665.

[66] Z. Li, G. Sun, M. Chen, S. Jin, X. Hao, C. Zhang, J. Ouyang, J. Zhu, B. Li, F. Cheng, Y. Xue, Evaluation of the radical scavenging potency and mechanism of natural phenolamides: a DFT study, J. Mol. Liq. 383 (2023) 122140, https://doi.org/10.1016/j.molliq.2023.122140.